Canadian Science Publishing

ARTICLE

$^{40}Ar/^{39}Ar$ dating of Paleoproterozoic shear zones in the Ellesmere–Devon crystalline terrane, Nunavut, Canadian Arctic

Brandon Caswell, Jane A. Gilotti, Laura E. Webb, William C. McClelland, Karolina Kośmińska, Karsten Piepjohn, and Werner von Gosen

Abstract: Paleoproterozoic gneisses of the Ellesmere–Devon crystalline terrane on southeastern Ellesmere Island are deformed by metre-scale, east-striking mylonite zones. The shear zones commonly offset pegmatitic dikes and represent the last episode of ductile deformation. Samples were dated by the $^{40}Ar/^{39}Ar$ step-heating method to put an upper limit on the time of deformation. Biotite from one tonalitic protolith and five shear zones give geologically meaningful results. Clusters of unoriented biotite grains pseudomorph granulite-facies orthopyroxene in some of the weakly deformed gneisses, whereas the shape-preferred orientation of biotite defines the mylonitic fabric. The intrusive age of the tonalitic protolith is 1958 ± 12 Ma, based on previous U–Pb dating of zircon. $^{40}Ar/^{39}Ar$ analysis of biotite from the same sample gave a plateau age of 1929 ± 23 Ma, which is interpreted as cooling from regional granulite facies metamorphism. Three nearby samples of mylonitic tonalite have $^{40}Ar/^{39}Ar$ ages in the range of ≈1870–1840 Ma. Biotite from two granitic mylonites over 80 km away return high-resolution Ar spectra in the same range, implying that widespread ductile shearing occurred at ≈1870–1840 Ma, or ≈90 million years after cooling from regional metamorphism. Although the 2.0–1.9 Ga gneisses of southeastern Ellesmere Island correlate with the Inglefield Mobile Belt in North-West Greenland and the Thelon Tectonic Zone, the late shear zones are superimposed on that juvenile arc long after the 1.97 Ga Thelon orogeny.

Key words: $^{40}Ar/^{39}Ar$ dating, biotite, Ellesmere Island, mylonite, shear zone.

Résumé : Des gneiss paléoprotérozoïques du terrane cristallin d'Ellesmere–Devon dans le sud-est de l'île d'Ellesmere sont déformés par des zones métriques de mylonites de direction Est. Dans bien des cas, ces zones de cisaillement ont entraîné le décalage de dykes de pegmatite et représentent le dernier épisode de déformation ductile. Des échantillons ont été datés au $^{40}Ar/^{39}Ar$ par la méthode de chauffe par paliers afin d'établir une limite d'âge supérieure pour la déformation. Des biotites provenant d'un protolite tonalitique et de cinq zones de cisaillement donnent des résultats cohérents du point de vue géologique. Des amas de grains de biotite sans orientation privilégiée représentent des pseudomorphes d'orthopyroxène du faciès des granulites dans certains des gneiss faiblement déformés, alors que l'orientation privilégiée d'autres grains de biotite définit la fabrique mylonitique. L'âge d'intrusion du protolite tonalitique est de 1958 ± 12 Ma, à la lumière de résultats passés de datation U–Pb sur zircons. L'analyse $^{40}Ar/^{39}Ar$ de biotite du même échantillon produit un âge de plateau de 1929 ± 23 Ma, qui est interprété comme étant l'âge du refroidissement ayant suivi le métamorphisme régional au faciès des granulites. Trois échantillons de tonalite mylonitique prélevés à proximité ont donné des âges $^{40}Ar/^{39}Ar$ dans l'intervalle de ≈1870–1840 Ma. De la biotite de deux mylonites granitiques situées à plus de 80 km donne des spectres de Ar de haute résolution dans la même fourchette d'âges, ce qui sous-entend qu'un cisaillement ductile répandu a eu lieu dans l'intervalle de ≈1870–1840 Ma, ou ≈90 millions d'années après le refroidissement qui a suivi le métamorphisme régional. Bien que les gneiss de 2,0–1,9 Ga du sud-est de l'île d'Ellesmere soient corrélés à la ceinture mobile d'Inglefield du Groenland du Nord-Ouest et à la zone tectonique de Thelon, les zones de cisaillement tardives ont été superposées sur cet arc juvénile bien après l'orogenèse de Thelon à 1,97 Ga. [Traduit par la Rédaction]

Mots-clés : datation $^{40}Ar/^{39}Ar$, biotite, île d'Ellesmere, mylonite, zone de cisaillement.

Introduction

The Laurentian craton is a collage of large Archean provinces separated by long, narrow, mostly Paleoproterozoic orogenic belts (Fig. 1; Hoffman 1988; Whitmeyer and Karlstrom 2007). The Thelon tectonic zone is the oldest and most northern orogen; it separates two Archean cratons, the Slave province from Rae province to the southeast (Hoffman 1988). The Thelon tectonic zone is an approximately 50–100 km wide accretionary orogen containing 2.0–1.9 Ga juvenile arc material that welds the older cratons together. To the southwest, similar Paleoproterozoic rocks, known as the Taltson magmatic belt, are offset by the Great Slave

Received 29 October 2020. Accepted 15 February 2021.

B. Caswell, J.A. Gilotti, and W.C. McClelland. Department of Earth and Environmental Sciences, University of Iowa City, IA 52240, USA.
L.E. Webb. Department of Geology, University of Vermont, Burlington, VT 05405, USA.
K. Kośmińska. Department of Earth and Environmental Sciences, University of Iowa City, IA 52240, USA; Faculty of Geology, Geophysics and Environmental Protection, AGH – University of Science and Technology, Kraków 30-059, Poland.
K. Piepjohn. Bundesanstalt für Geowissenschaften und Rohstoffe, Stilleweg 2, D-30655 Hannover, Germany.
W. von Gosen. Geozentrum Nordbayern, Krustendynamik, Friedrich-Alexander Universität Erlangen-Nürnberg, D-91054 Erlangen, Germany.
Corresponding author: Jane A. Gilotti (email: jane-gilotti@uiowa.edu).

Fig. 1. Map showing basement provinces of northern Laurentia. Archean cratons are shown in blue and Paleoproterozic orogenic belts are dark green, orange, and brown. BF, Bathurst fault; BH, Buffalo Head terrane; *BI,* Baffin Island; CB, Cumberland batholith; *DI,* Devon Island; *EI,* Ellesmere Island; GSLSZ, Great Slave lake shear zone; IMB, Inglefield Mobile Belt; WY, Wyoming Province. Map is modified from St-Onge et al. (2009) and Beranek et al. (2013).

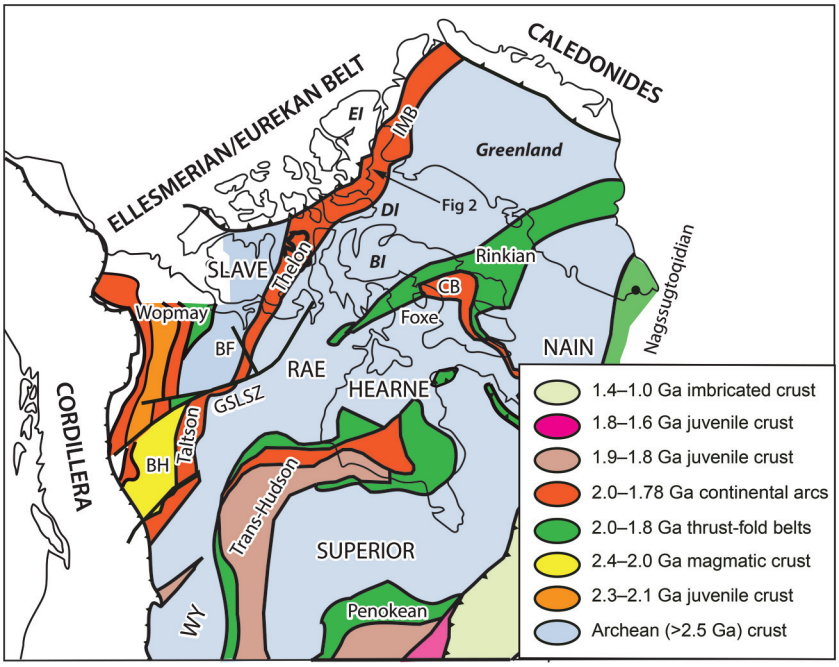

Lake shear zone and extend into Alberta and Saskatchewan (Hoffman 1987). The Taltson magmatic zone separates an amalgamation of mostly buried terranes in the west, such as the 2.4–2.0 Ga Buffalo Head terrane, from the Rae craton (Pehrsson et al. 2013). The Taltson arc initiated around 1.99 Ga with early I-type magmatism, which gave way to later collision-related S-type intrusions and granulite facies metamorphism that ended around 1.92 Ga (McDonough et al. 2000 and references therein). Card et al. (2014) caution against conflating the Taltson and Thelon orogenies due to detailed age differences, but for our purposes both are Paleoproterozoic arcs formed on the northwest boundary of the Rae craton.

A number of authors have suggested that the Thelon orogen extends to Ellesmere Island and into northwestern Greenland based on the presence of juvenile, 2.0–1.9 Ga Paleoproterozoic plutons that are candidates for subduction-related arc magmas (Fig. 1; Hoffman 1989; Nutman et al. 2008; St-Onge et al. 2009). The Ellesmere–Devon crystalline terrane (Fig. 2; Frisch 1988) is part of a Paleoproterozoic gneiss complex that forms the northeast portion of the Canadian Shield. Intrusive complexes with possible continental arc affinities range in age from 2.01 to 1.96 Ga (Frisch and Hunt 1988; Gilotti et al. 2018). This terrane is buried to the north by Phanerozoic sedimentary rocks of the Arctic platform, and juxtaposed against the Rae craton on Devon and Baffin Islands (cf. St-Onge et al. 2009). Paleoproterozoic basement rocks extend across Nares Strait to the northwest coast of Greenland, where they are referred to as the Inglefield Mobile Belt (Fig. 1; e.g., Dawes 1991). Nutman et al. (2008) defined two belts of juvenile magmatic arc rocks within the Inglefield Mobile Belt — a northern segment dominated by 1.95–1.92 Ga rocks and an older, 1.98 Ga area to the south. They also showed that the northernmost crystalline rocks in Greenland, near Victoria Fjord at 81°30′N, are Neoarchean. This is the first evidence of an Archean province located north of the Inglefield Mobile Belt that may be correlative with the Slave craton and, hence, lends further credence to the idea that the Thelon Tectonic zone can be extended northeastward.

In general, the timing of metamorphic and deformational events in southeastern Ellesmere Island and northwestern Greenland is poorly known. This contribution presents the first attempt to describe and date thin ductile shear zones that cut the Ellesmere–Devon crystalline terrane. Because the shear zones are the youngest and lowest grade ductile deformation features observed in this terrane, their age puts an upper limit on the time of metamorphism and deformation and helps with correlating these structures to events in Greenland, as well as the larger Thelon tectonic zone. To this end, we present a microstructural analysis of the mylonites in these shear zones and characterize the mineral chemistry of biotite to aid in interpretation of the Ar geochronology. We dated eight samples using a robust $^{40}Ar/^{39}Ar$ stepwise heating technique. Samples include biotite from a tonalitic protolith adjacent to a shear zone, six biotite-bearing samples from mylonites and white mica from a protolith pegmatite. The results show that the mylonite zones are Paleoproterozoic and overprint the Thelon orogen along its northeastern extension in Ellesmere Island.

Geologic setting

The Ellesmere–Devon crystalline terrane (Frisch 1988) is situated along the southeast margin of the Canadian Archipelago from 75°N to 79°N (Fig. 2). The oldest rocks are paragneisses with granulite-facies assemblages, including garnet + cordierite + sillimanite ± orthopyroxene schist, marble, and quartzite. Arc-related orthopyroxene-bearing tonalite, granodiorite, and granite intruded the paragneiss prior to high-grade metamorphism. A few U–Pb thermal ionization mass spectrometery (TIMS) dates of zircon (Frisch and Hunt 1988) record magmatic ages: a retrogressed granite gave a date of 1972 ± 41 Ma, an orthopyroxene-bearing granite was 1951 ± 12 Ma, and a tonalite was 1960 ± 5 Ma. Gilotti et al. (2018) produced U–Pb sensitive high-resolution ion microprobe – reverse geometry (SHRIMP-RG) ages for oscillatory-zoned zircon from an additional five samples. Three samples were metagranitoids that gave intrusive ages of 2007 ± 14, 2006 ± 21, and 1991 ± 8 Ma. One of these samples contained zircon with unzoned, cathodoluminescence-

Fig. 2. Geologic map of northwestern Greenland and adjacent Canada. The Paleoproterozoic rocks (pink), a probable extension of the Thelon tectonic zone, are called the Ellesmere–Devon crystalline terrane west of Nares Strait and the Inglefield Mobile Belt in Greenland. U–Pb ages from Ellesmere and Devon Islands are from Frisch and Hunt (1988) or Gilotti et al. (2018), and from Nutman et al. (2008) in Greenland. The star indicates the locality of the metamorphic ages from Frisch and Hunt (1988). VF, Victoria Fiord.

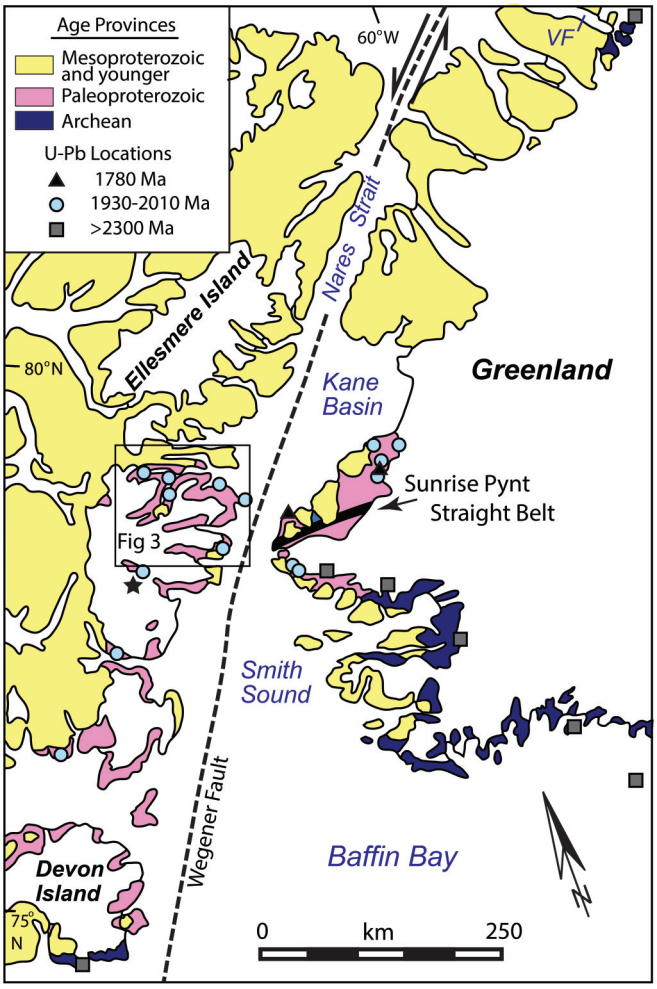

dark rims, which gave a lower intercept date of 357 ± 16 Ma, interpreted to be related to fluid ingress. A garnet-bearing granitic orthogneiss produced a date of 1977 ± 13 Ma. Lastly, a metatonalite resulted in a date of 1958 ± 12 Ma. The SHRIMP ages overlap with the earlier dates of Frisch and Hunt (1988), falling in the range of 2.0–1.9 Ga expected for subduction-related plutonism associated with a Thelon magmatic arc (Hoffman 1988). During deformation and metamorphism at granulite facies, metasedimentary rocks were partially melted to form peraluminous granites (Frisch 1988). Frisch and Hunt (1988) obtained U–Pb TIMS dates from zircon and monazite in garnet + cordierite bearing peraluminous granite of ca. 1960 and 1930 Ma, respectively. The dates are interpreted as the time of metamorphism because the granites are crustal melts formed during granulite-facies anatexis (Supplementary data file S1[1]; Frisch 1988). At present, these dates are the only constraint on the timing of metamorphism and deformation in the Ellesmere–Devon crystalline terrane.

Little structural work has been done on the polydeformed gneisses of the Ellesmere–Devon crystalline terrane. The terrane lies unconformably beneath subhorizontal sedimentary rocks of the late Precambrian Thule group and the Paleozoic shallow platform (Fig. 3). A predominantly north-striking regional gneissic fabric is approximately parallel to lithologic contacts (Frisch 1984). The gneissosity is moderately well developed in the paragneisses, but can be quite weak in the more massive intrusive rocks. The north-striking gneissosity on southeastern Ellesmere Island is at a high angle to the east–west gneissosity on Devon Island (Frisch 1984) and North-West Greenland (Dawes and Gaarde 2004; Nutman et al. 2008). A number of metre-scale mylonite zones were observed cutting the gneiss of the Ellesmere–Devon crystalline terrane. In contrast, a ductile shear zone up to 30 m thick has been reported on Devon Island (Frisch 1988), but was outside the area of our study. Large, steep brittle faults cut the basement and cover rocks, e.g., along Jokel Fiord (Harrison et al. 2009) and Hayes Fiord (Gilotti et al. 2018). Discrete populations of brittle fractures seen in nearly every outcrop may be related to motion on the Cenozoic Wegener fault and subsequent Eurekan contraction (von Gosen et al. 2019).

Methods

$^{40}Ar/^{39}Ar$ geochronology

$^{40}Ar/^{39}Ar$ analysis was performed at the University of Vermont Noble Gas Geochronology Laboratory in Burlington, Vermont, USA. Inclusion-free mineral grains were handpicked from eight samples after applying standard crushing and separation techniques. Samples were loaded into aluminum foil packets and irradiated with multigrain aliquots of Fish Canyon Tuff sanidine (28.201 Ma; Kuiper et al. 2008) to monitor the neutron dose. Ca and K salts were also irradiated to determine correction factors for interfering nuclear reactions. Samples were irradiated for 2 hours at the Cadmium-Lined In-Core Irradiation Tube facility at Oregon State University, Corvallis, Oregon, USA. The irradiation time was optimized for the possibility of Cenozoic mica ages.

Laser step-heating for $^{40}Ar/^{39}Ar$ dating was conducted with a Santa Cruz Laser Microfurnace 75 W diode laser system. With the exception of sanidine flux monitors and white mica, samples were loaded directly into wells in a copper sample holder. Sanidine and white mica grains were loaded into degassed Nb foil packets before being loaded in the wells in the sample holder. Single grains were analyzed for relatively coarse-grained gneisses and pegmatite; for very-fine-grained (ultra)mylonites, aliquots of 15–20 grains were analyzed. The gas released during heating was purified with SAES getters and argon isotopes were analyzed on a Nu Instruments Noblesse magnetic sector noble gas mass spectrometer in peak-hopping mode during step heating. Data from samples and flux monitors were corrected for blanks, mass discrimination, atmospheric argon, neutron-induced interfering isotopes, and the decay of ^{37}Ar and ^{39}Ar. Mass discrimination was calculated by analyzing known aliquots of atmospheric argon for which the measured $^{40}Ar/^{36}Ar$ was compared with an assumed atmospheric value of 298.56 (Lee et al. 2006). Correction factors used to account for interfering nuclear reactions are as follows: ($^{40}Ar/^{39}Ar$) K = $5.4 \times 10^{-4} \pm 1.4 \times 10^{-4}$ (Jicha and Brown 2014); ($^{36}Ar/^{37}Ar$) Ca = $2.65 \times 10^{-4} \pm 0.22 \times 10^{-4}$ and ($^{39}Ar/^{37}Ar$) Ca = $6.95 \times 10^{-4} \pm 0.09 \times 10^{-4}$ (Renne et al. 2013).

Ages were calculated using the isotope decay constants recommended by Min et al. (2000) and Stoenner et al. (1965). Inverse isochrons and apparent ages were calculated using both an in-house data reduction program and Isoplot 3.0 (Ludwig 2003). Weighted mean and plateau ages are reported following criteria reported by McDougall and Harrison (1999) and Schaen et al. (2021). A plateau age is calculated if four or more consecutive steps account

[1]Supplementary data are available with the article at https://doi.org/10.1139/cjes-2020-0197.

Fig. 3. Simplified geologic map of the northern Ellesmere–Devon crystalline terrane (pink), which is unconformably overlain by the Neoproterozoic Thule Group and Paleozoic rocks of the Arctic platform, showing Ar sample locations. Map modified from Frisch (1984) and contains information licensed under the Open Government License – Canada.

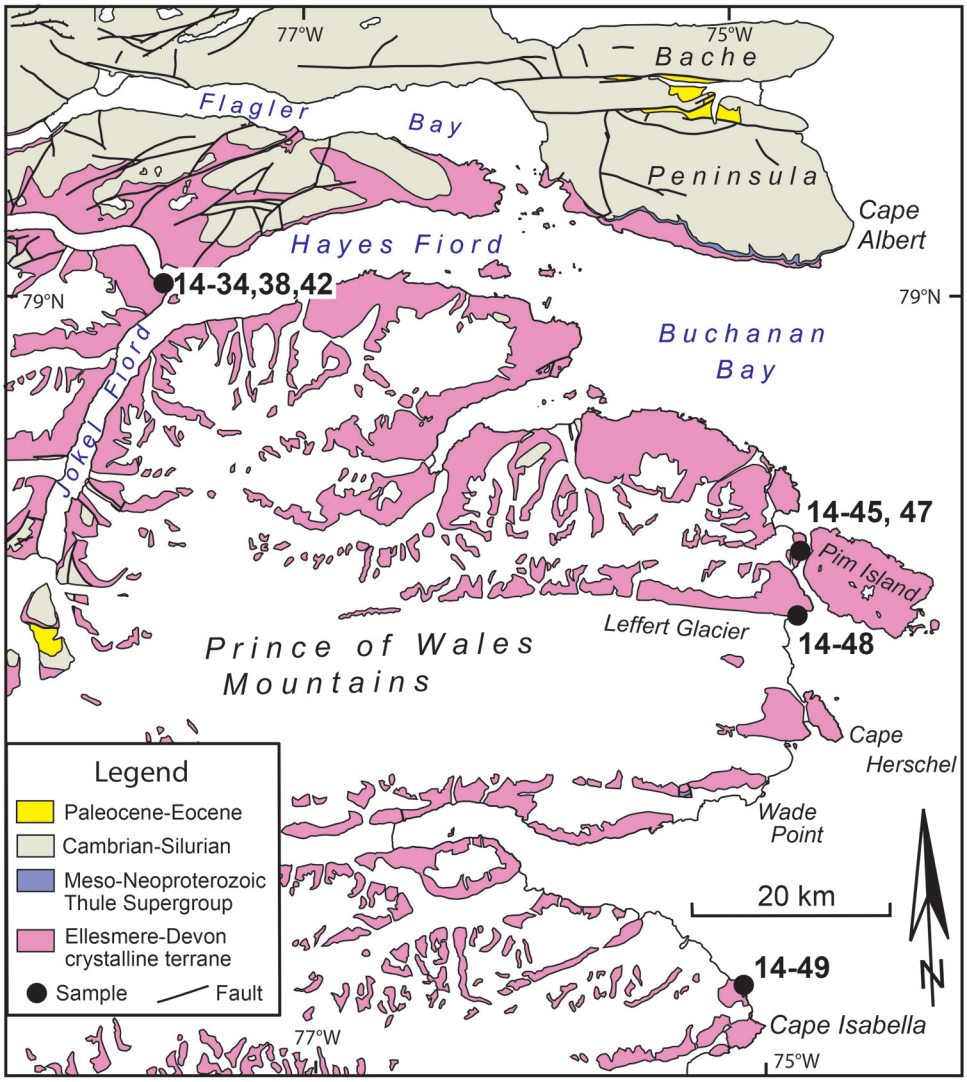

for 60% of cumulative ^{39}Ar released. Errors are quoted at the 1σ level and include precision associated with measurement of the irradiation parameter, J, for flux monitors.

Mineral chemistry

Biotite composition and major element zoning patterns were determined to characterize the mineral for Ar analysis. The mineral chemistry was obtained with the electron microprobe at the Department of Earth and Environmental Sciences, University of Iowa, Iowa, USA. Biotite was analyzed in standard polished thin sections on a JEOL JXA-8230 Superprobe operating in wavelength-dispersive spectrometry mode at 15 kV accelerating voltage and a current of 20 nA with the aid of backscattered-electron imaging. A total of 76 biotite grains were analyzed from four samples and representative compositions are shown in Supplementary data file S2[1].

Late shear zones of the Ellesmere–Devon crystalline terrane

Thin ductile shear zones (<1 m thick) are found locally throughout the Ellesmere–Devon crystalline terrane. The shear zones contain greenschist-facies protomylonites to ultramylonites and mark the latest plastic deformation of the rocks. Microstructures were studied in 17 thin sections of tectonites collected from tonalitic gneisses in western Hayes Fiord and metagranitoid gneisses along the southeast coast (Fig. 3). White mica from one pegmatite, biotite from one protolith gneiss, and six mylonites were chosen for Ar dating. Table 1 summarizes the ^{40}Ar/^{39}Ar results; the complete data set is presented in Supplementary data file S3[1].

Shear zones in metatonalite from Hayes Fiord

A weakly deformed metatonalite is cut by three prominent, thin ductile shear zones in an outcrop at the west end of Hayes Fiord (Fig. 4*a*). The shear zones are up to a few hundred metres long and < 1 m thick (Fig. 4*b*) and contain steeply dipping, east-northeast- to east-striking ductile mylonites (Fig. 4*c*). Stretching lineations defined by quartz and feldspar aggregates are shallowly plunging towards both the east and west. Kinematics are obvious in outcrop from displaced dikes (Fig. 4*d*), S-C fabrics, σ-porphyroclasts and (or) rotation of the mylonitic foliation into the shear zones (Supplementary data file S1[1]). The two northern shear zones are sinistral, while the southern one is dextral. In detail, the central shear zone is segmented into dominantly sinistral strands with offsets of a few metres of a prominent granitic

Table 1. Summary of $^{40}Ar/^{39}Ar$ results.

Sample	Lat (°N)	Long (°W)	Phase	PA (Ma)	WMA (Ma)	1σ	%^{39}Ar	MSWD	Prob.	TFA (Ma)
14-34	79.017959	77.664863	Biotite	—	1870 ± 16	11.1	45.4	0.6	0.83	1832.1
14-38a	79.018154	77.66717	Biotite	1845 ± 13	—	10.7	94.5	0.76	0.81	1818.6
14-38b	79.018154	77.66717	Biotite	1838 ± 14	—	12.2	99.3	0.79	0.72	1822.4
14-42	79.018154	77.66717	Biotite	1929 ± 23	—	23.1	95.9	1.6	0.097	1882.2
14-45	78.754532	74.7068	White mica	1977 ± 35	—	36.4	95.7	1.8	0.10	1979
14-47	78.754497	74.708179	Biotite	1874 ± 13	—	12.4	98.2	0.91	0.57	1852.1
14-48b	78.702090	74.718432	Biotite	1840 ± 11	—	8.1	95.8	0.54	0.98	1820.2
14-49a	78.364979	75.103047	Biotite	2051 ± 26	—	21.9	67.1	2	0.050	1992.8

Note: PA, plateau age if more than 3 steps with >60% released gas are concordant; WMA, weighted mean age if similar steps do not define a plateau; MSWD, mean square weighted deviation; Prob., probability of fit; TFA, total fusion age.

dike (Fig. 4*d*). We studied four samples from this area, shown in Fig. 4, including a protolith sampled within 1 m of the northernmost shear zone that returns a starkly different plateau age than the mylonites.

The protolith of the mylonites at the Hayes Fiord locality is a homogenous, weakly deformed metatonalite. The metatonalite consists of quartz, plagioclase, biotite, epidote/clinozoisite, amphibole, and ilmenite with accessory titanite and zircon. Biotite occurs in clots of randomly oriented grains (Fig. 5*a*) that Frisch (1988) interprets as replacing the granulite-facies orthopyroxene. No orthopyroxene was observed in our samples. Biotite is homogenous and slightly phlogopitic in composition, with X_{Fe} = 0.38–0.41. Most of the feldspar grain boundaries are strongly embayed, suggesting high-temperature grain boundary mobility consistent with the granulite-facies metamorphism. The minerals in the metatonalite do not exhibit a deformation fabric except close to the shear zones. We dated biotite from the clusters in sample 14-42, located 1 m to the right of the coin in Fig. 4*b*. The biotite produced an initial low-temperature step (minimum age) of 219 Ma followed by a step up to 1267 Ma and then to 1511 Ma. The remaining 95.9% of the cumulative ^{39}Ar released gave a plateau age of 1929 ± 23 Ma (Fig. 5*d*).

With increasing strain associated with the discrete shear zones, the biotite in the clusters takes on a strong grain-shaped preferred orientation, as seen in sample 14-34 (Fig. 5*b*). This sample has the same mineralogy as the protolith. Quartz shows mostly polygonal grain boundaries. Biotite, whose shape-preferred orientation defines the mylonitic foliation, gave an initial low-temperature step that resulted in a minimum date of 1205 Ma. The next 46% of ^{39}Ar released rose from 1760 to 1826 Ma, while 45.4% of the ^{39}Ar defines a weighted mean age of 1870 ± 16 Ma (Fig. 5*e*). Because the data did not define a plateau, the steps utilized in this calculation were selected based on visual identification of a plateau-like segment.

Sample 14-38 (Fig. 4*b*) displays extreme grain size reduction from a mylonitic fabric in 14-38a to an ultramylonite in 14-38b. The mylonite consists of quartz, K-feldspar, plagioclase, epidote, and biotite with accessory titanite, chlorite, zircon, and oxides. Its microstructure is very similar to mylonite 14-34 (Fig. 5*b*), where laths of olive green to yellow pleochroic biotite define the mylonitic foliation. Biotite is compositionally homogenous (Fig. 6) and its mineral chemistry is very similar to grains in the protolith clusters. The TiO_2 content fluctuates among mylonite samples up to 1.99 from 1.42 wt% in the protolith (14-42). Quartz is polygonal and devoid of any undulose extinction. A biotite mineral separate yields a minimum age of 1306 Ma, followed by a step up to 1735 Ma. A high-resolution plateau date (defined by 30 out of 32 total steps) of 1845 ± 13 Ma is associated with the remaining 94.5% of the ^{39}Ar released (Fig. 5*f*).

We also analyzed biotite from ultramylonite 14-38b, which is adjacent to 14-38a (Fig. 4*b*). The ultramylonite contains the same mineral assemblage; however, it is more fine grained and the phases are more evenly dispersed (Fig. 5*c*). Small (≈200 μm) grains of biotite pin quartz and feldspar grain boundaries creating a polygonal microstructure. Biotite gives a minimum date of 1433 Ma before stepping up to a well-defined plateau of 1838 ± 14 Ma defined by 99.34% of the ^{39}Ar released (Fig. 5*g*).

Shear zones in metagranitoids

Gneisses of granitic composition are quite common in the Ellesmere–Devon crystalline terrane (Frisch 1988). They were also metamorphosed in the granulite facies and polydeformed prior to the development of the late ductile shear zones. We observed a number of shear zones in coastal outcrops along Smith Sound (Fig. 3). The shear zones are commonly, although not always, localized around pegmatites and show progressive strain from protomylonite to mylonite to ultramylonite (Fig. 7). The three sampled shear zones dip moderately to steeply towards the north and have feldspar and quartz aggregate stretching lineations that plunge shallowly towards the southwest or shallowly to moderately towards the northeast. All kinematics are dextral based on the rotation of the gneissosity into parallelism with the shear zones. The shear zones are generally <1 m thick and could not be followed for more than tens of metres in length.

Sample 14-47 is a quartzofeldspathic augen mylonite (Fig. 7*a*; Supplementary data file S1[1]) from a thin (<1 m) shear zone in a retrogressed granitic gneiss located just west of Pim Island. The rock consists of quartz, plagioclase, K-feldspar, biotite, epidote, and ilmenite. The augen are single, polycrystalline and myrmekitic feldspar, as well as granitic lithic fragments. Biotite is very fine grained, defining the mylonitic foliation as well as late-stage shear bands (Fig. 8*a*). Quartz forms ribbons with undulose extinction, containing a range of blocky large subgrains to areas with small subgrains (Supplementary data file S4[1]) interpreted to form by bulging recrystallization (Stipp et al. 2002). A very-fine-grained matrix of quartz, biotite, and feldspar constitutes ≈50% of the rock. Biotite from this sample produces an initial low-temperature step that gives a minimum date of 1212 Ma, followed by the next step that produced a maximum date of 2009 Ma. The remaining 98.2% of ^{39}Ar gives a well-defined plateau age of 1874 ± 13 Ma (Fig. 8*b*).

Granitic mylonite sample 14-48b was collected from an outcrop (Fig. 7*b*) beneath the north wall of the Leffert Glacier. The mylonite is composed of quartz, plagioclase, K-feldspar, biotite, ilmenite, titanite, and late chlorite. Quartz forms coarse ribbons with serrated subgrain boundaries and undulose extinction, which together with biotite, define the mylonitic foliation (Fig. 8*c*). Feldspar augen exhibit coarse subgrains, consistent with the early high-temperature history of these rocks. Biotite is dominated by small (<200 μm), reddish brown pleochroic grains. Biotite is slightly more Fe-rich than the other samples, with X_{Fe} = 0.44–0.47, and more Ti-rich. Sample 14-48b had a biotite mineral separate that gave a high-resolution step-heated analysis resulting in a simple age spectra (Fig. 8*d*). An initial low-temperature step associated with only a few percent of the cumulative ^{39}Ar released resulted in an age of 1157 Ma. The next step jumped to 1760 Ma followed by a

Fig. 4 (*a*) Map of shear zones and samples at the west end of Hayes Fiord. ot, orthopyroxene tonalite; tg, biotite-orthopyroxene tonalite gneiss; ms, metasedimentary rocks (Frisch 1984). (*b*) Photograph of mylonite sample 14-38 in Shear Zone 1. Sample 14-42 of the weakly deformed protolith lies 1 m to the right of the coin. (*c*) Lower hemisphere, equal area stereographic projection of shear zone orientations (great circle), lineations (dot), and movement sense of hanging wall (arrow) for structures shown in Fig. 4*a*. (*d*) Detailed map of segmented shear zone showing offset of a single granitic dike, smaller dikelets (blue), and location of mylonite 14-34. [Color online.]

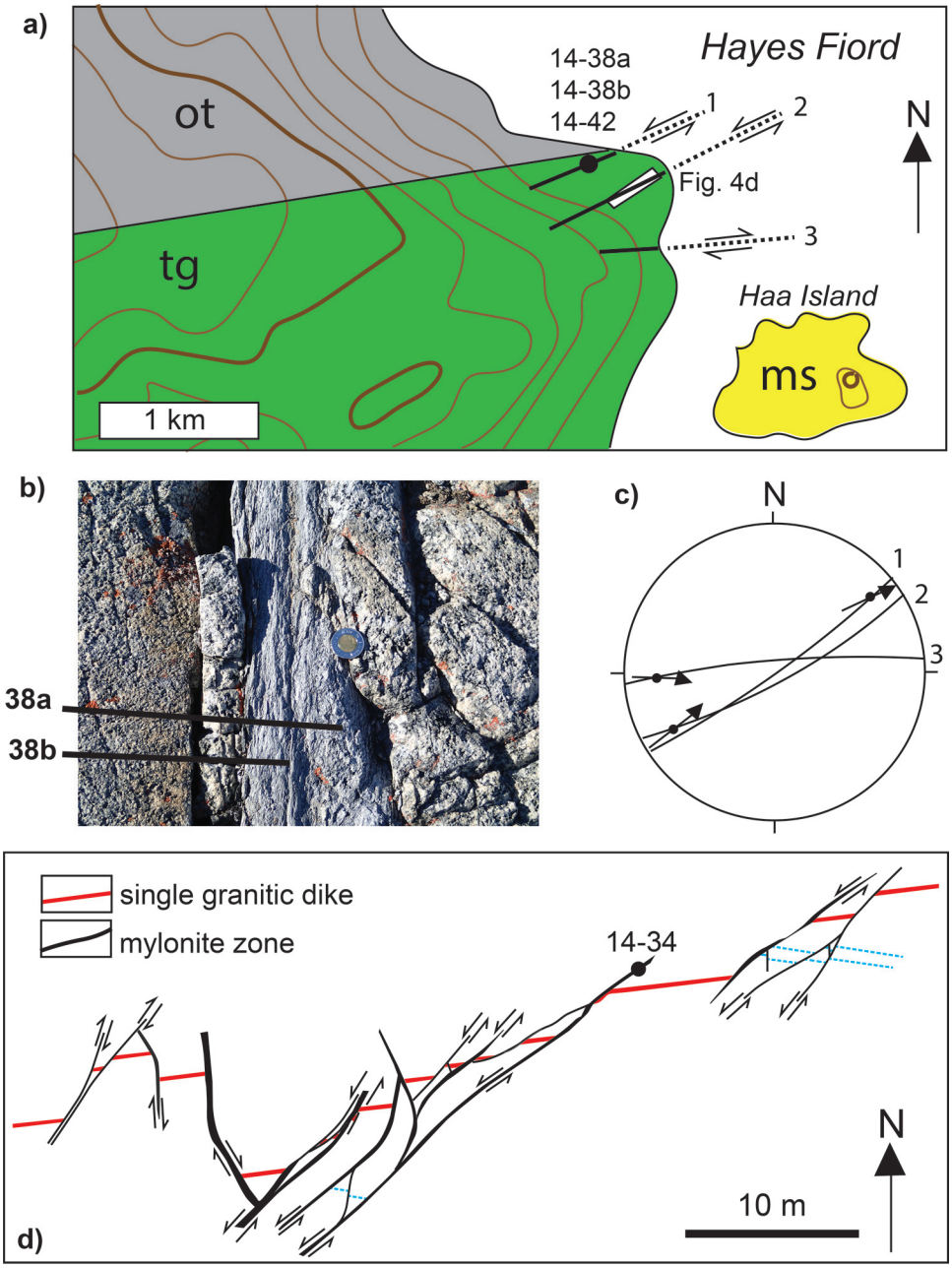

plateau age of 1840 ± 11 Ma over the remaining 95.8% of ^{39}Ar released.

Sample 14-49 is a mylonite from a deformed granitic pegmatite in a dextral shear zone (Fig. 7*c*) located approximately 4 km from Cape Isabella. The mylonite contains quartz, plagioclase, K-feldspar, biotite, garnet, oxides, and titanite. Quartz forms ribbons with undulose extinction and a range of subgrain types — from blocky to mostly amoeboid with irregular boundaries (Fig. 8*e*). Feldspar, biotite, and quartz are the main phases in the very-fine-grained matrix. Larger biotite overgrows garnet and defines the mylonitic foliation, while very fine biotite marks shear bands. A fine-grained biotite aliquot was step-heated resulting in a simple age spectrum (Fig. 8*f*). An initial low-temperature step associated with only a few percent of the cumulative ^{39}Ar released resulted in an age of 1072 Ma. The sample jumped to a plateau age of 2051 ± 26 Ma over the next 67.1% of ^{39}Ar release. Approximately 32% of the remaining ^{39}Ar released was divided between four steps. Although the data define a plateau based on standard criteria (i.e., four or more associated steps comprising ≥60% of cumulative ^{39}Ar released

Fig. 5. Cross-polarized light photomicrographs and Ar spectra of biotite in metatonalite from Hayes Fiord. Bt, biotite; Pl, plagioclase; Qz, quartz. (*a*) Biotite forms clusters surrounded by quartz and feldspar in undeformed metatonalite 14-42. (*b*) Biotite defines the mylonitic foliation in sample 14-34. (*c*) Small biotite grains have a strong grain-shaped preferred orientation in ultramylonite 14-38b. (*d–g*) $^{40}Ar/^{39}Ar$ stepwise-heating spectra for progressively deformed metatonalite. Boxes with darker tint were used for the age calculation; height of boxes is 1σ. [Color online.]

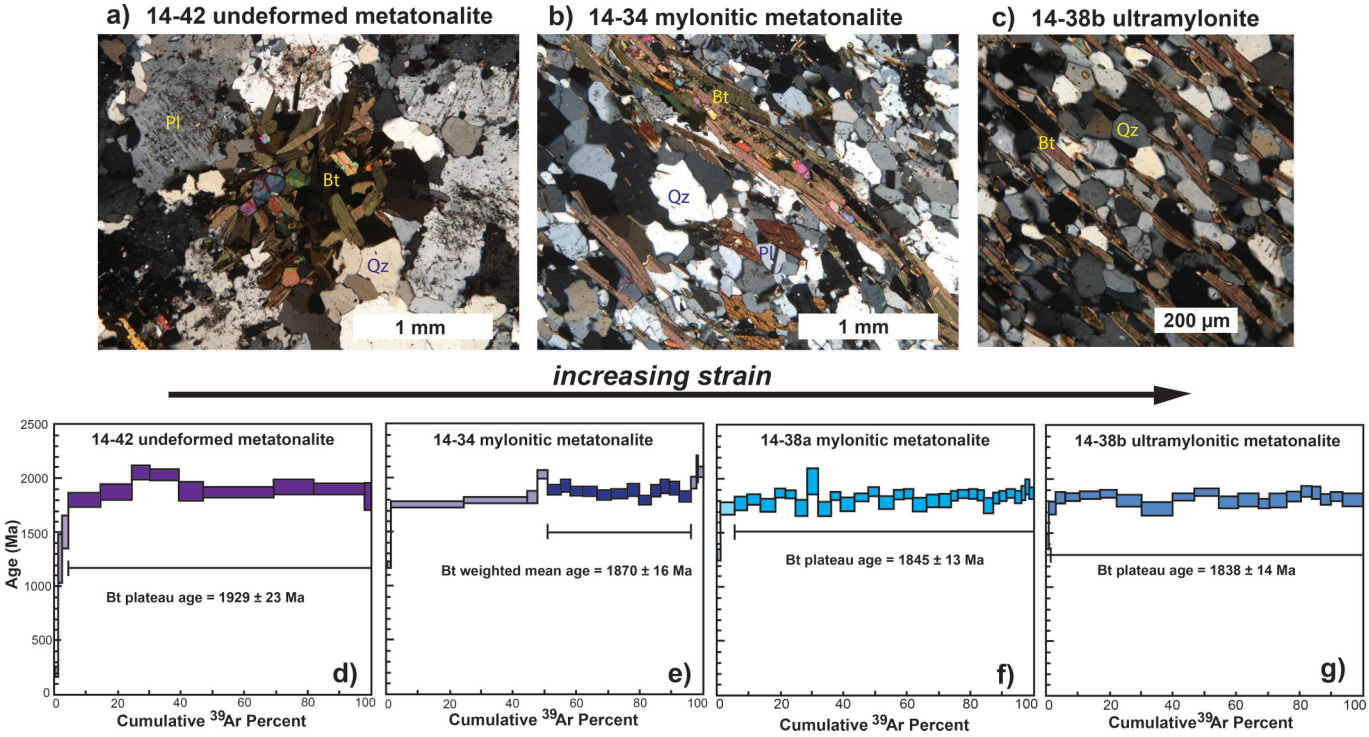

Fig. 6. Backscattered-electron images of biotite showing compositional homogeneity for mylonite samples 14-38a and 14-48b. Thin lamellae of chlorite are intergrown with biotite in 14-48b. Bt, biotite; Chl, chlorite; Ep, epidote; Kfs, K-feldspar; Pl, plagioclase; Qz, quartz.

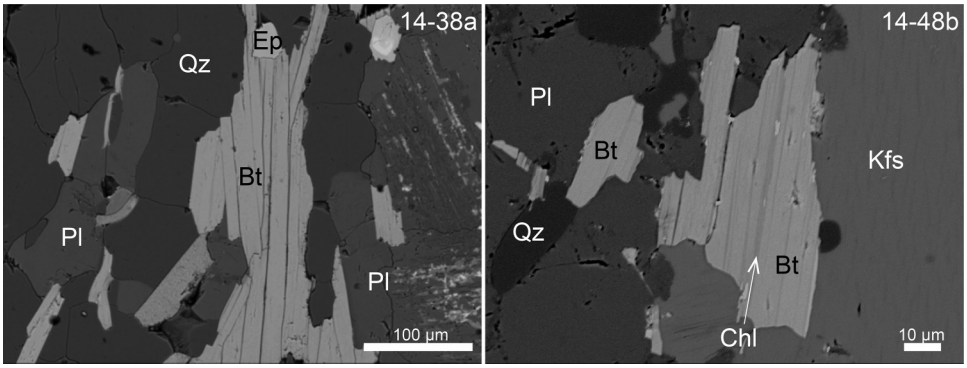

with ages concordant at the 2σ level), the resulting date is older than the oldest granite protolith identified by U–Pb dating (Gilotti et al. 2018), and is thus geologically uninterpretable.

Sample 14-45 was collected from a centimetre-sized white mica book in a granitic pegmatite within 100 m of sample 14-47 (Fig. 9*a*). The pegmatite consists of quartz, K-feldspar, plagioclase, biotite, and white mica with accessory zircon, chlorite, and opaque minerals. The step-heated white mica immediately jumped to a plateau date of 1997 ± 35 Ma for the first 95.7% of ^{39}Ar released (Fig. 9*b*). The final step gives a maximum age of 2312 Ma. Although the plateau age seems possible as the time of intrusion of the pegmatite, it does not fit with a metamorphic history that saw temperatures in excess of 800 °C during granulite facies metamorphism after 1960 Ma. For this reason, we interpret the 1997 Ma plateau age as geologically meaningless.

Discussion

$^{40}Ar/^{39}Ar$ results reflect timing of deformation

$^{40}Ar/^{39}Ar$ stepwise heating of micas has been used to successfully date the time of mylonitization in ductile shear zones (e.g., Costa and Maluski 1988; Dunlap et al. 1991; Goodwin and Renne 1991; Webb et al. 2010; Klepeis et al. 2019). Because micas can dynamically recrystallize and grow during deformation at temperatures below their nominal closure temperature (Kirschner et al. 1996; Dunlap 1997), direct dating of low-grade mylonites is possible. Incomplete recrystallization of mica porphyroclasts in

Fig. 7. Photographs of shear zones in granitoids. (*a*) Mylonite 14-47 shows gradation from protomylonite (PM) at pen to black augen mylonite (AM). (*b*) Gneissosity at hammer wraps into a dextral shear zone (SZ); sample 14-48b is from this shear zone. (*c*) Shear zone (SZ) northwest of Cape Isabella shows dextral offset (sample 14-49) above deformed pegmatite (at coin). (*d*) Lower hemisphere, equal area stereonets of these shear zones with same symbols as Fig. 4*c*. [Color online.]

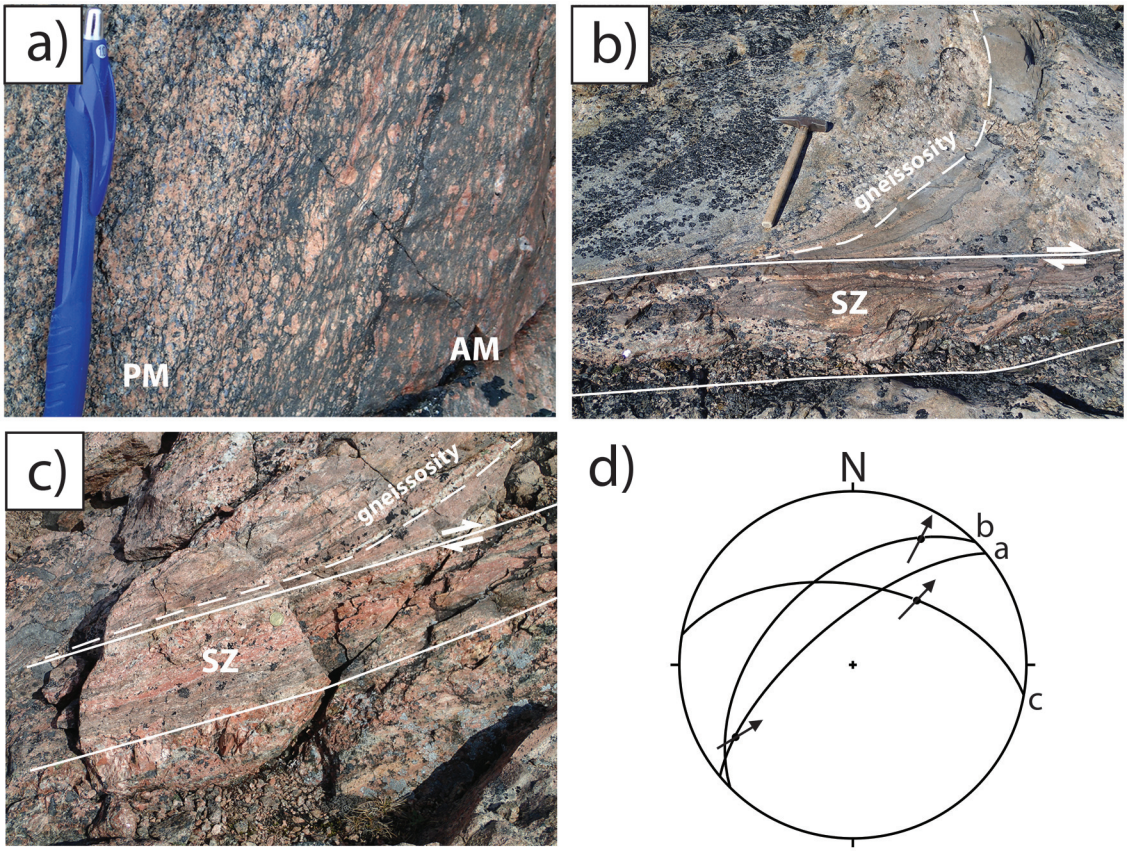

mylonites can be detected by in situ ultraviolet-laser techniques (Mulch and Cosca 2004) and be associated with highly discordant apparent age spectra (Mulch et al. 2002), but robust plateau dates indicate simple isotope systematics (Schaen et al. 2021) of an individual grain.

Our $^{40}Ar/^{39}Ar$ study targets late shear zones and utilizes the concept that this isotope system can be reset at temperatures near or below biotite closing temperature to date a specific deformation event. We dated biotite in seven samples to establish the timing of widespread thin ductile shear zones from the Ellesmere–Devon crystalline terrane. The very fine biotite grain sizes of the mylonite and ultramylonite samples precluded the ability to analyze single grains in these samples; however, the lack of porphyroclastic textures and compositional zoning for biotite suggest homogeneous populations. A large number of steps — in two cases, over 30 — were measured to capture any possible Cenozoic history that may have been related to the Wegener Fault (Gilotti et al. 2018; von Gosen et al. 2019). The results are high-resolution spectra of Paleoproterozoic dates, with all but one sample giving a plateau age.

The outcrop at the west end of Hayes Fiord gives a coherent picture of the late shear zones. The protolith of the metatonalite was emplaced at 1958 ± 12 Ma (mean square weighted deviation = 1.2), based on a weighted mean $^{207}Pb/^{206}Pb$ age from high-U, oscillatory-zoned zircon (Gilotti et al. 2018). Biotite from the same sample gives a $^{40}Ar/^{39}Ar$ plateau date of 1929 ± 23 Ma (Fig. 5). The biotite forms retrograde clusters that replace granulite-facies orthopyroxene (Frisch 1988); thus, the $^{40}Ar/^{39}Ar$ age reflects cooling from the granulite-facies metamorphism. In contrast, a mylonite and ultramylonite from a thin shear zone 1 m from the dated protolith (Fig. 4*b*) have biotite plateau dates of 1845 ± 13 and 1838 ± 14 Ma, respectively. The Ar spectrum of biotite from a mylonite in a different shear zone at Hayes Fiord, sample 14-34 (Fig. 4), is not as well equilibrated as 14-38a and 14-38b. It gives a weighted mean date of 1870 ± 16 Ma from 12 steps representing 45.4% of the cumulative ^{39}Ar released. The close proximity of the cooled metatonalite at ≈1930 Ma and the younger mylonites ≈60–90 million years later is strong evidence that the Ar system in biotite was reset by localized deformation in the shear zones. An alternative interpretation, which we do not favor, is that the plateau date from the metatonalite is somehow flawed (e.g., by excess Ar) and the dates from the mylonites are cooling ages. Shear zones located 80 km southeast of the Hayes Fiord locality return similar $^{40}Ar/^{39}Ar$ ages. A granitic mylonite near Pim Island yields a biotite plateau date of 1874 ± 13 Ma, while biotite from a sample near the north wall of the Leffert Glacier gives a plateau date of 1840 ± 11 Ma. The reproducibility of the dates over considerable distance demonstrates that the late shear zones belong to a single generation.

The greenschist-facies mylonites in this study overprint granulite-facies gneisses such that many feldspar and quartz porphyroclasts still retain evidence of high-temperature microstructures; therefore, progressive, retrograde deformation makes it difficult to use quartz microstructures to estimate temperature. For example, grain boundary mobility, seen as embayed boundaries in some of the coarser quartz ribbons (14-49, Fig. 8*e*), probably formed during granulite-facies metamorphism. In contrast, the serrated quartz subgrain boundaries in mylonite 14-48 (Fig. 8*c*) are indicative of

Fig. 8. Cross-polarized light photomicrographs and Ar spectra with box height of 1σ for granitic mylonites. Boxes with lighter tint were not used in the age calculations. (*a*) Very-fine-grained biotite surrounding quartz ribbon with fine subgrains in granitic mylonite 14-47 and (*b*) corresponding biotite stepwise heating spectra. (*c*) Quartzofeldspathic mylonite 14-48b with fine-grained biotite outlining quartz ribbons with blocky subgrains and (*d*) biotite Ar spectra. (*e*) Mylonite 14-49 showing biotite parallel to mylonitic foliation defined by quartz ribbons. Arrows mark biotite in extremely fine-grained shear bands. (*f*) Ar spectra for biotite for 14-49. See Supplementary data file S4[1] for corresponding plane light photomicrographs that highlight biotite. [Color online.]

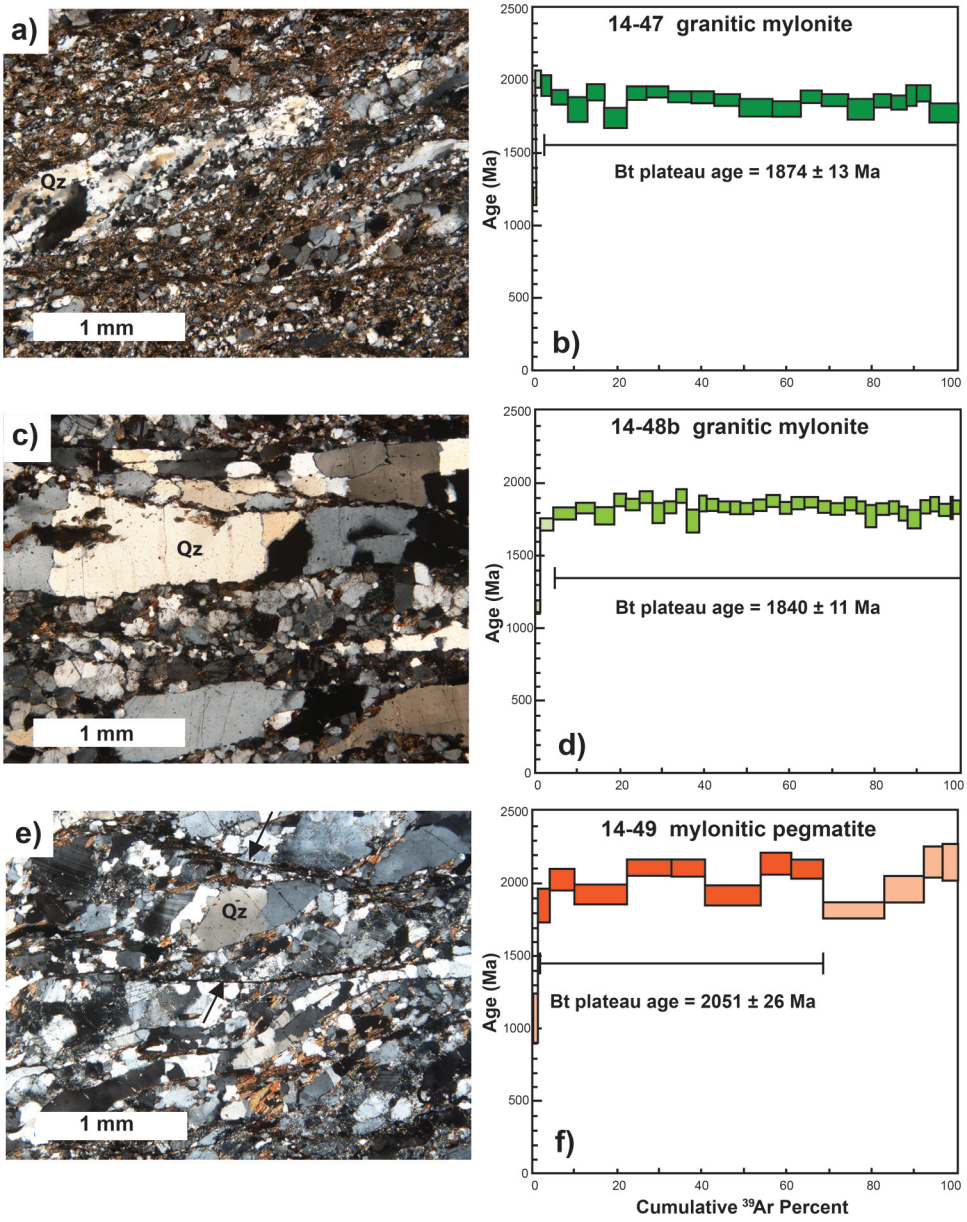

bulging recrystallization (>280 °C), while patchy mosaics of small subgrains in 14-47 (Supplementary data file S4[1]) suggest subgrain rotation recrystallization (>400 °C; Stipp et al. 2002). However, the main strain-producing mechanism is likely fluid-assisted, low-temperature diffusion creep in the fine-grained groundmass (Gilotti 1992), where biotite is conceivably still growing or recrystallizing. The polygonal quartz in the metatonalitic mylonites (14-34, 14-38a, and 14-38b) could be interpreted as static recrystallization after grain boundary migration recrystallization at 500 °C or biotite may pin the quartz grain boundaries as it grows at low temperature. Dunlap (1997) describes a similar scenario for white mica and quartz mylonites deformed at <350 °C. The fact that greenschist-facies mylonites with a broad array of microstructures give the same age over a large area supports our interpretation that the ^{40}Ar/^{39}Ar system dates deformation.

Some of the granitic samples contain chlorite intergrowths in biotite (Fig. 6). An increasing degree of chloritization can produce disturbed age spectra with hump-shaped patterns due to a mixed release of ^{39}Ar from submicrometre scale biotite and chlorite interlayers (Lo and Onstott 1989; Di Vincenzo et al. 2003). Curved release patterns were not observed in the apparent age spectra from our samples, which implies fairly simple systematics or fortuitous avoidance of chlorite-rich domains in biotite.

^{40}Ar/^{39}Ar plateau ages do not preclude excess Ar (e.g., Schertl and Hammerschmidt 2016); but in this case, good control on the geochronology by other isotopic systems is critical to the

Fig. 9 (*a*) Photograph of granitic pegmatite sample 14-45. The arrow points to centimetre-scale white mica. (*b*) Ar spectra for white mica from pegmatite shown in Fig. 9*a*. [Color online.]

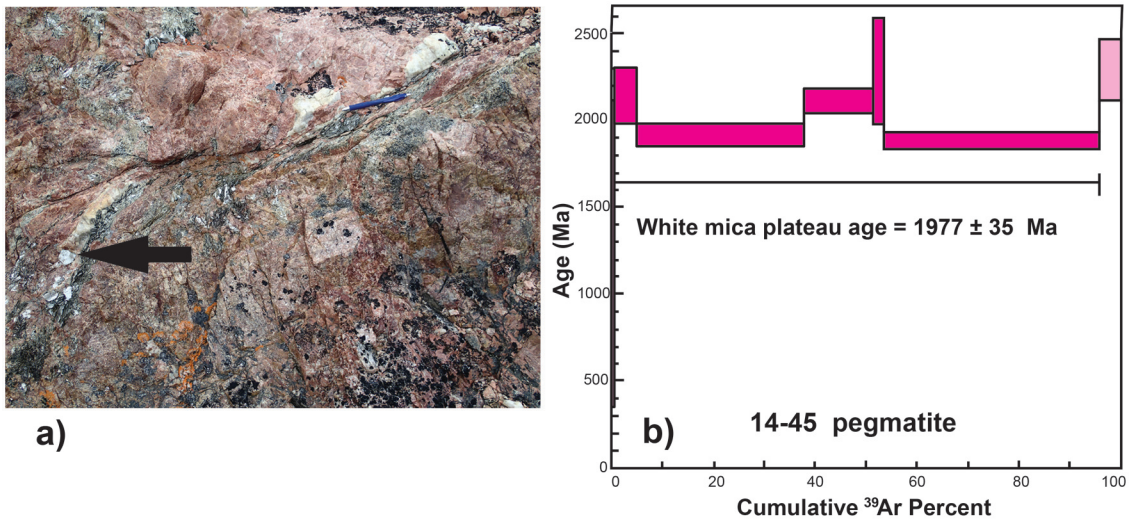

interpretation. We determined that two samples yield plateau dates that are older than the known geologic context based on U–Pb dating of the orthogneisses. (1) A mylonitic pegmatite from the southernmost shear zone (14-49) gave a biotite plateau age of 2051 ± 26 Ma, which is older than the oldest intrusive age of Paleoproterozoic granitoids at 2007 ± 14 Ma (Gilotti et al. 2018). (2) White mica from a pegmatite (14-45) defined a plateau age of 1977 ± 35 Ma, which is younger than the intrusive age of the gneissic protoliths but older than the age of metamorphism at 1960–1930 Ma (Frisch and Hunt 1988). We would expect this white mica to record the cooling age from granulite facies similar to sample 14-42, but it appears to suffer from excess Ar. By virtue of the age of the samples, the radiogenic ^{40}Ar (^{40}Ar*) components are generally >99% for most steps (see Supplementary data file S3[1]), rendering the inverse isochron data to cluster in a ball rather than a mixing line between trapped and radiogenic argon components that would allow us to evaluate the data for excess argon.

Regional significance

The Precambrian geologic history of the Ellesmere–Devon crystalline terrane is complex and the timing of metamorphic and deformational events is poorly known. Polydeformed metasedimentary rocks were intruded by a suite of granitoids, granodiorites, and tonalites with an age range of ≈2.0–1.95 Ga (Frisch and Hunt 1988; Gilotti et al. 2018). Similar intrusive suites are interpreted to represent arc-related plutons associated with subduction leading to collision of the Slave and Rae cratons (Whalen et al. 2018 and references therein). The contrast between the intrusives with weak metamorphic fabrics, such as the metatonalite at Hayes Fiord (Fig. 4*b*), and the strongly deformed paragneisses suggests either some deformation prior to arc plutonism or heterogeneous strain. Regional granulite-facies metamorphism (Frisch 1988) led to melting of pelitic paragneiss (Supplementary data file S1[1]) and is inferred to record collision. The age of metamorphism is poorly constrained by U–Pb TIMS dates of 1960 Ma on zircon and 1930 Ma on monazite from anatectic melts (Frisch and Hunt 1988). Our ^{40}Ar/^{39}Ar plateau age of 1929 ± 23 Ma from biotite replacing orthopyroxene in sample 14-42 shows that the metatonalites had cooled through the closure temperature of biotite by ≈1930 Ma — typically quoted as ≈300 °C (Grove and Harrison 1996) but possibly as high as ≈450 °C with higher phlogopite and halogen compositions (Grove 1993) — and pushes the age of granulite facies metamorphism somewhat older. Modern petrochronology is needed to better understand the complicated pressure–temperature–time–deformation evolution of the granulite facies metamorphism and is beyond the scope of this work.

The mylonite zones described in this paper are the youngest ductile structures observed cutting the gneisses of the Ellesmere–Devon crystalline terrane. We obtained consistent ^{40}Ar/^{39}Ar stepwise heating results of ca. 1870–1840 Ma from biotite in five out of six mylonite samples, where four of the dates are well-defined plateaus. The mylonite zones cut metatonalites that cooled to or through lower greenschist-facies conditions at 1930 Ma, indicating that they formed during an unrelated event beginning at least 60 million years after the formation and metamorphism of the Paleoproterozoic arc. Frisch (1988) describes a larger east-striking shear zone on Devon Island, which is an obvious target for future work. Are the mylonites dated here related to this structure? If they are, then the accretionary boundary between the Paleoproterozoic arc and Archean gneisses of the Rae craton to the south must be an older structure than the late shear zones.

Similar Paleoproterozoic gneisses are found across Nares Strait in Greenland in the Inglefield Mobile Belt (Fig. 2). Nutman et al. (2008) combine cathodoluminescence imaging and U–Pb SHRIMP dating of zircon to delineate a northern, younger belt of arc intrusives at 1950–1940 Ma from older, southern plutonism at 2000–1980 Ma. Sm–Nd model ages on the same samples support their interpretation that the Inglefield Mobile Belt is dominated by a juvenile Paleoproterozoic arc. The northern and southern segments of the arc are separated by a steep east-striking, high-strain zone about 10 km wide, known as the Sunrise Pynt Straight Belt. According to these authors, this high-temperature deformation zone lacks mylonites and is younger than 1800 Ma. The Sunrise Pynt Straight Belt does not continue westward to Ellesmere Island, where the metamorphic fabric is oriented north–south (Frisch 1984), but may be offset southward to Devon Island across Kane Basin (Gilotti et al. 2018). Protolith ages of orthogneisses on Ellesmere Island best match Nutman et al.'s (2008) ca. 2.0–1.98 Ga gneisses south of the Sunrise Pynt Straight Belt. Our ^{40}Ar/^{39}Ar biotite ages from low-grade mylonite zones suggests that the Sunrise Pynt Straight Belt is probably older than 1870 Ma and unrelated to the late mylonite zones. Although we assert that the shear zones dated here at 1870–1840 Ma are the youngest ductile deformation event seen on southeastern Ellesmere Island, we do so with caution and acknowledge that more work is needed to understand the Precambrian history. For example, Nutman et al. (2008) produced U–Pb zircon dates for three granitoids north of

the Sunrise Pynt Straight Belt of 1783 ± 22, 1752 ± 25, and 1741 ± 41 Ma and describe the rocks as having gneissic fabrics. We have not recognized this suite of granites in the Ellesmere–Devon crystalline terrane.

Kellett et al. (2020) recently reviewed the cooling history of the Thelon tectonic zone (TTZ) within a framework of northwest-directed convergence of the Slave and Rae cratons at approximately 1.97 Ga (Tirrul and Grotzinger 1990), followed by indentation of the Slave into the Rae before 1.84 Ga (Ma et al. 2020). Hornblende $^{40}Ar/^{39}Ar$ dates indicate cooling through ≈500 °C at 1.89–1.87 Ga in the central TTZ migrating to 1.83–1.80 Ga in the southwest, while biotite cooled through ≈ 290 °C at 1.80–1.78 Ga across the zone. The TTZ is displaced by the sinistral Bathurst fault during the late indentation phase (Hoffman 1988). Monazite dates show that ductile fabrics formed from 1933 to 1895 Ma, while biotite cooling at 1840 Ma marks the beginning of brittle deformation (Ma et al. 2020) along the Bathurst fault.

The discrete shear zones dated on Ellesmere Island at 1870–1840 Ma are clearly younger than the collision marked by the Thelon orogeny. They fit within the time frame of later deformation associated with adjustments during the amalgamation of the supercontinent Nuna, such as the documented indentation of the Slave into the Rae craton (Ma et al. 2020) and reworking of the Rae province (Pehrsson et al. 2013; Kellett et al. 2020).

Acknowledgements

This project was supported by a National Science Foundation EAGER grant (EAR-1432970) to J.A. Gilotti. Student grants to B. Caswell from the University of Iowa are gratefully acknowledged. The German Research Foundation (DFG Go 405-12/1) enabled the work of W. von Gosen. The German Federal Institute for Geosciences and Natural Resources organized and funded the logistics for the 2014 fieldwork. We thank the Nunavut government and Inuit communities for permission to work on Ellesmere Island, and we thank field guides Debby and Pilipossie Iqaluk and the Polar Continental Shelf Program for assistance with logistics. We are grateful to J.C. Harrison (Geological Survey of Canada) for encouraging us to study the late shear zones, D.A. Jones for his help with mineral separation and lab instruction during B. Caswell's visit to the University of Vermont, and K. Horkley for help with scanning electron microscope and electron microprobe data acquisition at the University of Iowa. The comments of two anonymous reviewers improved the manuscript.

References

Beranek, L.P., Pease, V., Scott, R.A., and Thomsen, T.B. 2013. Detrital zircon geochronology of Ediacaran to Cambrian deep-water strata of the Franklinian basin, northern Ellesmere Island, Nunavut: implications for regional stratigraphic correlations. Canadian Journal of Earth Sciences, **50**(10): 1007–1018. doi:10.1139/cjes-2013-0026.

Card, C.D., Bethune, K.M., Davis, W.J., Rayner, N., A., and K.E. 2014. The case for a distinct Taltson orogeny: Evidence from northwest Saskatchewan. Precambrian Research, **255**: 245–265. doi:10.1016/j.precamres.2014.09.022.

Costa, S., and Maluski, H. 1988. Use of the ^{40}Ar-^{39}Ar Stepwise heating method for dating mylonite zones: An example from the St. Barthélémy Massif (Northern Pyrenees, France). Chemical Geology, **72**: 127–144. doi:10.1016/0012-821X(93)90241-Z.

Dawes, P.R. 1991. Geological map of Greenland 1:500,000, Thule, Sheet 5: Geological Survey of. Denmark and Greenland. Copenhagen, Denmark.

Dawes, P.R., and Gaarde, A.A. 2004. Geological map of Greenland 1:500,000, Humbolt Gletscher, sheet 6. *In* Geological survey of Denmark and Greenland, Copenhagen, Denmark.

Di Vincenzo, G., Viti, C., and Rocchi, S. 2003. The effect of chlorite interlayering on ^{40}Ar–^{39}Ar biotite dating: an ^{40}Ar–^{39}Ar laser-probe and TEM investigations of variably chloritised biotites. Contributions to Mineralogy and Petrology, **145**: 643–658. doi:10.1007/s00410-003-0472-z.

Dunlap, W.J., Teyssier, C., McDougall, I., and Baldwin, S. 1991. Age of deformation of K/Ar and $^{40}Ar/^{39}Ar$ dating of white micas. Geology, **19**: 1213–1216. doi:10.1130/0091-7613(1991)019<1213:AODFKA>2.3.CO;2.

Dunlap, W.J. 1997. Neocrystallization or cooling? $^{40}Ar/^{39}Ar$ ages of white micas from low-grade mylonites. Chemical Geology, **143**: 181–203. doi:10.1016/S0009-2541(97)00113-7.

Frisch, T. 1984. Geology, Prince of Wales Mountains, District of Franklin, Northwest Territories. Geological Survey of Canada. Map 1572a, 1: 250–000.

Frisch, T. 1988. Reconnaissance geology of the Precambrian shield of Ellesmere, Devon and Coburg Islands, Canadian Arctic Archipelago. Geological Survey of Canada Memoir 409. 104pp.

Frisch, T., and Hunt, P.A. 1988. U–Pb zircon and monazite ages from the Precambrian shield of Ellesmere and Devon Islands, Arctic Archipelago. *In* Radiogenic age and isotopic studies. Report 2, Geological Survey of Canada Paper 88-2. pp. 117–125.

Gilotti, J.A. 1992. The rheologically critical matrix in arkosic mylonites along the Särv thrust, Swedish Caledonides. *In* Structural geology of fold and thrust belts. *Edited by* S. Mitra and G. Fisher. Johns Hopkins University Press, Baltimore, Md. pp. 145–160.

Gilotti, J.A., McClelland, W.C., Piepjohn, K., and von Gosen, W. 2018. U–Pb geochronology of Paleoproterozoic gneiss from southeastern Ellesmere Island: Implications for displacement estimates on the Wegener Fault. Arktos, **4**: 1–18. doi:10.1007/s41063-018-0047-x.

Goodwin, L.B., and Renne, P.R. 1991. Effects of progressive mylonitization on Ar retention in biotites from the Santa Rosa mylonite zone, California, and thermochronologic implications. Contributions to Mineralogy and Petrology, **108**: 283–297. doi:10.1007/BF00285937.

Grove, M., 1993. Thermal histories of southern California basement terranes. Ph.D. dissertation, University of California, Los Angeles, California.

Grove, M., and Harrison, T.M. 1996. $^{40}Ar^*$ diffusion in Fe-rich biotite. American Mineralogist, **81**: 940–951. doi:10.2138/am-1996-7-816.

Harrison, J.C., Thorsteinsson, R., and de Freitas, T.A. 2009. Phanerozoic bedrock geology, Strathcona Fiord area, Ellesmere Island, Nunavut. Geological Survey of Canada, Map 2141A, 1: 25–000.

Hoffman, P.F. 1987. Continental transform tectonics: Great Slave Lake shear zone (ca. 1.9 Ga), northwest Canada. Geology, **15**: 785–788. doi:10.1130/0091-7613(1987)15<785:CTTGSL>2.0.CO;2.

Hoffman, P.F. 1988. The United Plates of America, The Birth of a Craton: Early Proterozoic Assembly and Growth of Laurentia. Annual Reviews of Earth and Planetary Sciences, **16**: 543–603. doi:10.1146/annurev.ea.16.050188.002551.

Hoffman, P.F. 1989. Precambrian geology and tectonic history of North America. *In* The geology of North America—an overview. *Edited by* A.W. Bally and A.R. Palmer. Geological Society of America, Boulder, Colo., The Geology of North America v. A. pp. 447–512.

Jicha, B.R., and Brown, F.H. 2014. An age for the Korath Range, Ethiopia and the viability of $^{40}Ar/^{39}Ar$ dating of kaersutite in Late Pleistocene volcanics. Quaternary Geology, **21**: 53–57.s. doi:10.1016/j.quageo.2013.03.007.

Kellett, D.A., Pehrsson, S., Skipton, D.R., Regis, D., Camacho, A., Schneider, D.A., and Berman, R. 2020. Thermochronological history of the Northern Canadian Shield. Precambrian Research, **342**: 105703

Kirschner, D.L., Cosca, M.A., Masson, H., and Hunziker, J.C. 1996. Staircase $^{40}Ar/^{39}Ar$ spectra of fine-grained white mica: Timing and duration of deformation and empirical constraints on argon diffusion. Geology, **24**: 747–750. doi:10.1130/0091-7613(1996)024<0747:SAASOF>2.3.CO;2.

Klepeis, K.A., Webb, L.E., Blatchford, H.J., Jongens, R., Turnbull, R.E., and Schwartz, J.J. 2019. The age and origin of Miocene-Pliocene fault reactivations in the upper plate of an incipient subduction zone, Puysegur Margin, New Zealand. Tectonics, **38**: 3237–3260. doi:10.1029/2019TC005674.

Kuiper, K.F., Deino, A., Hilgen, F.J., Krijgsman, W., Renne, P.R., and Wijbrans, A.J. 2008. Synchronizing rock clocks of Earth history. Science, **320**(5875): 500–504. doi:10.1126/science.1154339. PMID:18436783.

Lee, J.Y., Marti, K., Severinghaus, J.P., Kawamura, K., Yoo, H.S., Lee, J.B., and Kim, J.S. 2006. A redetermination of the isotopic abundances of atmospheric Ar. Geochimica, et Cosmochimica Acta, **70**: 4507–4512. doi:10.1016/j.gca.2006.06.1563.

Lo, C.-H., and Onstott, T.C. 1989. ^{39}Ar recoil artifacts in chloritized biotite. Geochimica et Cosmochimica Acta, **53**: 2697–2711. doi:10.1016/0016-7037(89)90141-5.

Ludwig, K.R. 2003. User's manual for Isoplot 3.00, a geochronological toolkit for Microsoft Excel. Berkeley Geochronology Center Special Publication, USA. 72pp.

Ma, S.M., Kellett, D.A., Godin, L., and Jercinovic, M.J. 2020. Localisation of the brittle Bathurst fault on pre-existing fabrics: a case for structural inheritance in the northeastern Slave craton, western Nunavut, Canada. Canadian Journal of Earth Sciences, **57**(6): 725–746. doi:10.1139/cjes-2019-0100.

McDonough, M.R., McNicoll, V.J., Schetselaar, E.M., and Grover, T.M. 2000. Geochronological and kinematic constraints on crustal shortening and escape in a two-sided, oblique-slip collisional and magmatic orogeny, Paleoproterozoic Taltson magmatic zone, northeastern Alberta. Canadian Journal of Earth Sciences, **37**(11): 1549–1573. doi:10.1139/e00-089.

McDougall, I., and Harrison, T.M. 1999. Geochronology and thermochronology by the $^{40}Ar/^{39}Ar$ method. Oxford University Press, U.K.

Min, K., Mundil, R., Renne, P.R., and Ludwig, K.R. 2000. A test for systematic errors in $^{40}Ar/^{39}Ar$ geochronology through comparison with U/Pb analysis of a 1.1 Ga rhyolite. Geochimica, et Cosmochimica Acta, **64**: 73–98. doi:10.1016/S0016-7037(99)00204-5.

Mulch, A., and Cosca, M.A. 2004. Recrystallization or cooling ages: in situ UV-laser $^{40}Ar/^{39}Ar$ geochronology of muscovite in mylonitic rocks. Journal of the Geological Society, London, **161**: 573–582. doi:10.1144/0016-764903-110.

Mulch, A., Cosca, M., and Handy, M. 2002. In-situ UV-laser $^{40}Ar/^{39}Ar$ geochronology of a micaceous mylonite: an example of defect-enhanced argon loss. Contributions to Mineralogy and Petrology, **142**: 738–752. doi:10.1007/s00410-001-0325-6.

Nutman, A.P., Dawes, P.R., Kalsbeek, F., and Hamilton, M.A. 2008. Palaeoproterozoic and Archaean gneiss complexes in northern Greenland: Palaeoproterozoic terrane assembly in the High Arctic. Precambrian Research, **161**: 419–451. doi:10.1016/j.precamres.2007.09.006.

Pehrsson, S.J., Berman, R.G., and Davis, W.J. 2013. Palaeoproterozoic orogenesis during Nuna aggregation: A case study of reworking of the Rae craton, Woodburn Lake, Nunavut. Precambrian Research, **232**: 167–188. doi:10.1016/j.precamres.2013.02.010.

Renne, P.R., Deino, A.L., Hilgen, F.J., Kuiper, K.F., Mark, D.F., Mitchell, I.I.I., et al. 2013. Time scales of critical events around the Cretaceous-Paleogene boundary. Science, **339**: 684–687. doi:10.1126/science.1230492. PMID:23393261.

Schaen, A.J., IV., Jicha, B.R., Hodges, K.V., Vermeesch, P., Stelten, M.E., Mercer, C.M., et al. 2021. Interpreting and reporting $^{40}Ar/^{39}Ar$ geochronologic data. Geological Society of America Bulletin, **133**: 461–487. doi:10.1130/B35560.1.

Schertl, H.-P., and Hammerschmidt, K. 2016. Tracking the incidence of excess argon in white mica Ar–Ar data from UHP conditions to upper crustal levels in the Dora-Maira Massif, Western Alps. European Journal of Mineralogy, **28**: 1255–1275. doi:10.1127/ejm/2016/0028-2613.

Stipp, M., Stünitz, H., Heilbronner, R., and Schmid, S. 2002. The eastern Tonale fault zone: a 'natural laboratory' for crystal plastic deformation of quartz over a temperature range from 250 to 700°C. Journal of Structural Geology, **24**: 1861–1884. doi:10.1016/S0191-8141(02)00035-4.

Stoenner, R.W., Schaeffer, O.A., and Katcoff, S. 1965. Half-lives of argon-37, argon-39, and argon-42. Science, **148**(3675): 1325–1328. doi:10.1126/science.148.3675.1325. PMID:17791262.

St-Onge, M.R., Van Gool, J.A.M., Garde, A.A., and Scott, D.J. 2009. Correlation of Archaean and Palaeoproterozoic units between northeastern Canada and western Greenland: constraining the pre-collisional upper plate accretionary history of the Trans-Hudson orogeny. Geological Society, London, Special Publications, **318**: 193–235. doi:10.1144/SP318.7.

Tirrul, R., and Grotzinger, J.P. 1990. Early Proterozoic collisional orogeny along the northern Thelon tectonic zone, Northwest Territories, Canada: Evidence from the foreland. Tectonics, 9: 1015–1036. doi:10.1029/TC009i005p01015.

von Gosen, W., Piepjohn, K., Gilotti, J.A., McClelland, W.C., and Reinhardt, L. 2019. Structural evidence for sinistral displacement on the Wegener Fault in southern Nares Strait, Arctic Canada. *In* Circum-Arctic Structural Events: Tectonic evolution of the Arctic margins and trans-Arctic links with adjacent orogens. *Edited by* K. Piepjohn, J. Strauss, L. Reinhardt, and W.C. McClelland. Geological Society of America Special Paper 541. pp. 367–396.

Webb, L.E., Johnson, C.L., and Minjin, C. 2010. Late Triassic sinistral shear in the East Gobi Fault Zone, Mongolia. Tectonophysics, **459**: 246–255. doi:10.1016/j.tecto.2010.09.033.

Whalen, J.B., Berman, R.G., Davis, W.J., Sanborn-Barrie, M., and Nadeau, L. 2018. Bedrock geochemistry of the central Thelon Tectonic Zone, Nunavut. Geological Survey of Canada. Open File, 823449p, doi:10.4095/306385.

Whitmeyer, S.J., and Karlstrom, K.E. 2007. Tectonic model for the Proterozoic growth of North America. Geosphere, **3**: 220–259. doi:10.1130/GES00055.1.